

Low anisotropy of the upper critical field in a strongly anisotropic layered cuprate $\text{Bi}_{2.15}\text{Sr}_{1.9}\text{CuO}_{6+\delta}$: Evidence for a paramagnetically limited superconductivity.

S. O. Katterwe^{†,1}, Th. Jacobs,¹ A. Maljuk,² and V. M. Krasnov^{1*}

¹*Department of Physics, Stockholm University, AlbaNova University Center, SE-10691 Stockholm, Sweden*

²*Leibniz Institute for Solid State and Materials Research IFW Dresden, Helmholtzstr. 20, D-01171 Dresden, Germany*

(Dated: February 28, 2022)

We study angular-dependent magnetoresistance in a low T_c layered cuprate $\text{Bi}_{2.15}\text{Sr}_{1.9}\text{CuO}_{6+\delta}$. The low $T_c \sim 4$ K allows complete suppression of superconductivity by modest magnetic fields and facilitate accurate analysis of the upper critical field H_{c2} . We observe an universal exponential decay of fluctuation conductivity in a broad range of temperatures above T_c and propose a new method for extraction of $H_{c2}(T)$ from the scaling analysis of the fluctuation conductivity at $T > T_c$. Our main result is observation of a surprisingly low H_{c2} anisotropy ~ 2 , which is much smaller than the effective mass anisotropy of the material ~ 300 . We show that the anisotropy is decreasing with increasing field and saturates at a small value when the field reaches the paramagnetic limit. We argue that the dramatic discrepancy of high field and low field anisotropies is a clear evidence for paramagnetically limited superconductivity.

PACS numbers: 74.72.Gh 74.55.+v 74.72.Kf 74.62.-c

INTRODUCTION

The upper critical field H_{c2} is one of the key parameters of type-II superconductors [1]. It is particularly important for understanding unconventional superconductivity [2, 3]. However, estimation of H_{c2} for high-temperature superconductors is a notoriously difficult task. The high T_c leads to an extended region of thermally activated flux-flow. The complex physics of anisotropic pinning and melting of the vortex lattice [4] makes it hard, if at all possible [5], to confidently obtain H_{c2} from flux-flow characteristics at $T < T_c(H)$.

The high T_c in combination with a strong coupling leads to a large superconducting energy gap $\Delta \sim 20 - 50$ meV [6–11] and $H_{c2}(0) \sim 10^2$ T [12–19]. Such strong fields may alter the ground state of the material. For cuprates and pnictides the parent state is antiferromagnetic. It has been demonstrated that relatively weak fields can induce a canted ferromagnetic order in strongly underdoped cuprates [20]. Furthermore, the normal state of underdoped cuprates is characterised by the presence of the pseudogap (PG), which probably represents a charge/spin or orbital density wave order coexisting and competing with superconductivity [8, 10, 21–28]. Suppression of superconductivity by magnetic field may enhance the competing PG, as follows from observation of a charge density wave in a vortex core [9]. But even stronger magnetic fields of several hundred tesla suppress the PG [29, 30]. Thus, both superconducting and normal state properties are affected by strong magnetic fields and separation of the two contributions is highly non-trivial and controversial. Disentanglement of superconducting and PG characteristics is difficult even above T_c due to presence of profound superconducting fluctuations [31–33]. Therefore, principal new questions, which do not appear for low- T_c superconductors, are to

what extent $H \sim H_{c2}$ alters the abnormal normal state of high- T_c superconductors and how to define the non-superconducting background in measured characteristics.

For many unconventional superconductors the measured H_{c2} exceeds the paramagnetic limit of the BCS theory [1, 34]. This has been reported for organic [35–37], cuprate [14, 15], pnictide [38–40] and heavy fermion [41–43] superconductors. Such an overshooting is an important hint in a long standing search for exotic spin-triplet and Fulde-Ferrell-Larkin-Ovchinnikov states (for review see e.g. Ref.[43]). Yet, the overshooting is not a proof of unconventional pairing because the paramagnetic limit is rather flexible. It is increasing in the presence of spin-orbit interaction [1] and in the two-dimensional (2D) case and is lifted in the one-dimensional (1D) case [43, 44]. Unconventional superconductors are usually anisotropic. Some of them have quasi-2D, or possibly even quasi-1D structure. Many have a significant spin-orbit interaction between localized spins and itinerant charge carriers. Consequently, one needs a more robust criterion for the paramagnetically (un)limited superconductivity in search for exotic states of matter.

Here we investigate the anisotropy of H_{c2} in a strongly anisotropic layered $\text{Bi}_{2.15}\text{Sr}_{1.9}\text{CuO}_{6+\delta}$ (Bi-2201) cuprate with a low $T_c \sim 4$ K. The low T_c and the associated large disparity of superconducting and pseudogap scales [30] allow simple and accurate estimation of H_{c2} without complications typical for high- T_c cuprates. We present a detailed analysis of angular dependence of in-plane and out-of-plane magnetoresistances (MR) and demonstrate that they exhibit very different behavior. We observe an universal approximately exponential decay of the in-plane fluctuation para-conductivity above T_c and propose a method for extraction of $H_{c2}(T)$ from a new type of a scaling analysis of fluctuations at $T > T_c$. It obviates the complexity of the flux-flow phenomena and

allows unambiguous extraction of $H_{c2}(T)$. Remarkably, we obtained that the anisotropy of the upper critical field $H_{c2}^{\parallel}/H_{c2}^{\perp}(T \rightarrow 0) \simeq 2$ is much smaller than the anisotropy of the effective mass $\gamma_m \simeq 300$ [45]. This discrepancy clearly indicates that H_{c2}^{\parallel} parallel to the CuO planes is cut-off by the paramagnetic limit.

Cuprates have homologous families with different number of CuO planes per unit cell. Cuprates within the homologous family have similar carrier concentrations, resistivities, anisotropies and layeredness, but largely different T_c . For Bi-based cuprates the three-layer compound $\text{Bi}_2\text{Sr}_2\text{Ca}_2\text{Cu}_3\text{O}_{10+\delta}$ (Bi-2223) has a maximum T_c of ~ 110 K, the two-layer compound $\text{Bi}_2\text{Sr}_2\text{CaCu}_2\text{O}_{8+\delta}$ (Bi-2212) has a $T_c \sim 95$ K and a single-layer compound $\text{Bi}_2\text{Sr}_2\text{CuO}_{6+\delta}$ (Bi-2201) has an optimal (with respect to Oxygen doping) T_c that ranges from ~ 30 K for Bi/Pb and Sr/La substituted crystals [46] to just few K in the pure Bi-2201 compound [5, 47–49]. According to Ref. [48] the stoichiometric Bi-2201 compound is non-superconducting and a finite T_c appears only in off-stoichiometric $\text{Bi}_{2+x}\text{Sr}_{2-y}\text{CuO}_{6+\delta}$ compounds with $x, y \neq 0$. Thus, the Bi/Sr off-stoichiometry allows fine tuning of the maximum T_c [48, 49].

Development of high magnetic field techniques in recent years has lead to a significant progress in studies of H_{c2} in high- T_c superconductors [13, 14, 18, 19]. But the problem of disentanglement of superconducting and PG magnetic responses remains. It leads to a lack of clear criteria for extraction of H_{c2} from measurement at $H \sim 100$ T. This problem is avoided in low- T_c cuprates because the relative disparity between superconducting and pseudogap scales is increasing with decreasing T_c [30]. Therefore, analysis of H_{c2} in low- T_c cuprates should provide an unambiguous information about the superconducting state, not affected by interference with the co-existing PG. This is the main motivation of the present work.

EXPERIMENTAL

Studied crystals are parts of one pristine $\text{Bi}_{2.15}\text{Sr}_{1.9}\text{CuO}_{6+\delta}$ single crystal with $T_c \simeq 3.5$ K. Growth and characterization of crystals is described in Ref. [48]. Oxygen doping was consecutively decreased by soft annealing in vacuum, which does not affect the crystal quality [47]. We present data for a slightly overdoped (with respect to oxygen content) $T_c \simeq 4.0$ K [OD(4.0)] and a nearly optimally doped $T_c \simeq 4.3$ K [OP(4.3)] crystals.

Figure 1 (a) shows an image of the studied sample OP(4.3). The sample consists of ten micron-size mesa structures (two big and eight small) with attached gold electrodes. In-plane resistance is measured with a lock-in technique in a four-probe configuration by sending an accurate current through the left and right current contacts (big mesas), and measuring the longitudinal voltage between

a pair of small mesas. The c -axis transport is measured in a three-probe configuration by sending a probe current through one of the small mesas to one of the current contacts. The voltage is measured with respect to unbiased contact pad. Details of sample fabrication and measurement setup can be found in Ref. [30].

Fig. 1 (b) shows the c -axis resistance versus temperature at $H = 0$ and 14 T along the c -axis. It is seen that $R_c(T)$ exhibits an upturn at $T < T^* \sim 110$ K, indicating opening of the c -axis PG. According to previous studies [30, 46, 50] such a T^* corresponds to a near optimally doped (OP) (slightly underdoped) Bi-2201. A superconducting transition occurs at a much lower $T_c \simeq 4$ K. The c -axis field of 14 T completely suppresses the superconducting transition but does not change significantly the PG characteristics due to a large disparity of superconducting and PG scales in this low- T_c compound [30].

The large c -axis resistance $R_c \sim k\Omega$ corresponds to a non-metallic resistivity $\rho_c \simeq 20 \Omega\text{cm}$ [30], which is much larger than the in-plane resistivity $\rho_{ab} \simeq 1 - 4 \cdot 10^{-4} \Omega\text{cm}$ [51]. The anisotropy of resistivity $\gamma_R = \rho_c/\rho_{ab} \sim 10^5$ and the corresponding effective mass anisotropy $\gamma_m = \sqrt{\gamma_R} \sim 300$ is very large [45], similar to Bi-2212 [52] and Bi-2223 [53] cuprates. This reflects a layered 2D structure of Bi-based cuprates with mobile electrons localized on atomic CuO planes. The c -axis transport is caused by interlayer tunneling. Below T_c this leads to appearance of an intrinsic Josephson effect [54], observed in all Bi-based cuprates [6, 8, 16, 53, 55], including Bi-2201 [30, 50, 56]. Interlayer tunneling creates the basis for the intrinsic tunneling spectroscopy technique [6, 8, 16, 30, 53] and facilitates simultaneous magneto-transport and spectroscopic measurements, beneficial for analysis of H_{c2} [16]. Fig. 1 (c) shows the current-voltage I - V characteristics of a small mesa at $T = 1.8$ K. A detailed analysis of intrinsic tunneling characteristics of our Bi-2201 crystals can be found in Ref. [30]. Small area of our mesas allows investigation of intrinsic tunneling characteristics [6, 8, 16, 30, 53] without significant distortion by self-heating [8].

IN-PLANE AND OUT-OF-PLAIN MAGNETORESISTANCE

A. In-plane magnetoresistance

Figures 2 (a) and (b) show temperature dependencies of the in-plane resistance R_{ab} at different magnetic fields (a) perpendicular and (b) parallel to the ab planes for the OP(4.3) sample. For $H \perp ab$, R_{ab} reaches the normal state value R_n already at $H \simeq 10$ T. For $H \parallel ab$ the field of 17 T still does not completely suppress superconductivity. The difference is both due to the anisotropy and due to different contributions from flux-flow and orbital effects. The Lorentz force density $f_L = (1/c)[J \times B]$, where J is the transport current density and B is the

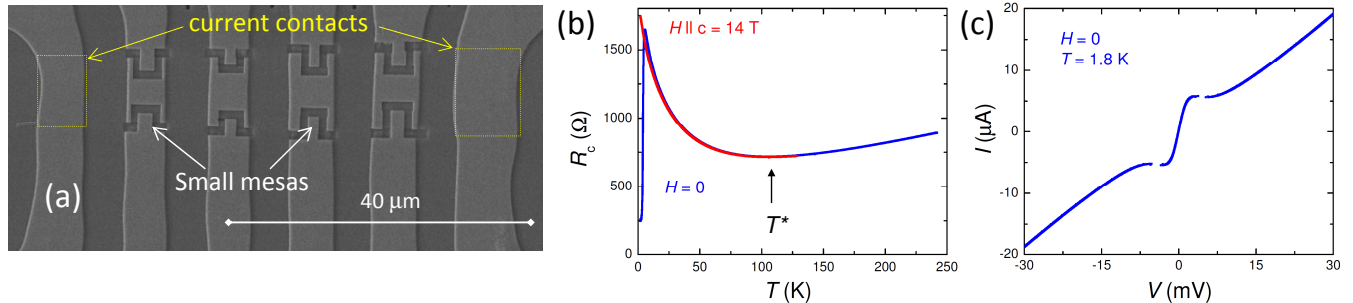


FIG. 1. (color online) (a) Scanning electron microscopy image of the sample OP(4.3). (b) Temperatures dependence of the c -axis resistance at $H = 0$ and 14 T. The compound has a low $T_c \simeq 4$ K and the pseudogap onset temperature $T^* \simeq 110$ K. (c) Current-voltage characteristic of a small mesa at $T = 1.8$ K and $H = 0$.

magnetic induction, acts both on vortices and mobile charge carriers. In Fig. 2 (a) $H \perp I \parallel ab$ the Lorentz force is at maximum and effectively drives pancake vortices [4] along CuO planes. Therefore, $R_{ab}(H \perp ab)$ is dominated by the flux-flow contribution at $T < T_c(H)$. In case of Fig. 2 (b) $H \parallel ab \parallel I$ there is no Lorentz force and the flux-flow contribution should be minimal.

Fig. 2 (c) represents a detailed comparison of $R_{ab}(T)$ at $H = 0$ and 17 T for the two field orientations. We notice that the resistive transition at $H \parallel ab \parallel I$ is simply shifted towards a lower T due to suppression of $T_c(H)$. On the other hand R_{ab} at $H \perp ab$ is also shifted upwards, even at $T \gg T_c$. It indicates that there is an additional positive MR in the normal state ($\sim 1\%$ at $H \perp ab = 17$ T). Thus, there are two different mechanisms of positive in-plane MR. At $T \lesssim T_c$ it is mostly due to suppression of superconductivity. Such MR saturates at $H \sim H_{c2}$. Fig. 2 (d) shows field-dependence of $R_{ab}(H^\perp)$ at $T = 1.8$ K and at $T = 4.2$ K $\sim T_c$. It is seen that saturation of $R_{ab}(H^\perp)$ occurs at significantly lower field for $T = 4.2$ K, consistent with reduction of H_{c2} at $T \rightarrow T_c$. In the normal state $T > T_c$ the tendency is reversed. With increasing T the saturation field is increasing. This can be seen from Figs. 2 (e) and (f), which show field-dependence of R_{ab} in perpendicular (circles) and parallel (squares) magnetic fields at $T = 2$ K and 7.7 K, respectively. Such behavior can be partly attributed to superconducting fluctuations, for which the characteristic field is increasing with $|T_c - T|$ [33]. However, fluctuations do not explain the increment of the saturation value of R_n , which is visible at $T \gg T_c$ and is significant only for $H \perp ab$, see Fig. 2 (c). Consequently, there is an additional normal state MR, caused by orbiting of mobile electrons in magnetic field [57]. This leads to a positive MR with saturation at $\omega_c \tau > 1$, where $\omega_c = eB/mc$ is the cyclotron frequency and τ is the scattering time. Since τ becomes shorter with increasing T , the saturation field is increasing with increasing T . Due to the quasi-2D electronic structure of Bi-2201, the orbital MR should appear only at $H \perp ab$, consistent with our observation.

B. Out-of-plane magnetoresistance

Figure 3 (a) and (b) show temperature dependencies of the c -axis resistance R_c at different magnetic fields (a) perpendicular and (b) parallel to the ab planes. Irrespective of field orientation, there are both positive and negative contributions to c -axis MR. Fig. 3 (c) represents a detailed comparison of $R_c(T)$ at $H = 0$ and at $H = 17$ T for the two field orientations. It is seen that in the normal state there is a significant negative c -axis MR for both field orientations. It is largest for $H \perp ab$ and reaches almost 10% in 17 T field.

A positive MR appears only in the superconducting state $T < T_c(H)$. It is due to suppression of the interlayer Josephson current with respect to the bias current [58, 59]. At $H \parallel ab$ there is a profound Josephson flux-flow phenomenon due to easy sliding of Josephson vortices along the ab -planes [55, 60]. This also leads to a positive MR with a peak at H strictly parallel to the ab -planes [61]. The negative c -axis MR persists both in the superconducting [16] and the normal states and is attributed to field suppression of either the superconducting gap Δ [16] or the pseudogap Δ_{PG} [29]. For high- T_c Bi-2212 [6, 8] and Bi-2223 [53] cuprates the corresponding energies ($\Delta \sim 30 - 50$ meV, $\Delta_{PG} \sim 30 - 70$ meV) and fields ($H_{c2} \sim 100 - 200$ T, $H^* \sim 200 - 300$ T) are similar [16, 29] and separation of the two contributions is difficult. However, in the studied low- T_c superconductor the separation becomes trivial because, as shown in Ref. [30], all PG characteristics remain similar to high- T_c materials, but all superconducting characteristics scale down with T_c [11], leading to a large disparity of superconducting and PG characteristics.

Figs. 3 (d,e) show c -axis MR for different field orientations and temperatures (d) below and (e) above T_c . It is seen that the negative MR persists at $H > H_{c2}^\perp \sim 10$ T and at $T > T_c$ and is due to field suppression of the PG [29, 30]. Fig. 3 (f) shows pulsed field measurements of $R_c(H^\perp)$ at $T = 1.6$ K up to 65 T for a slightly under-

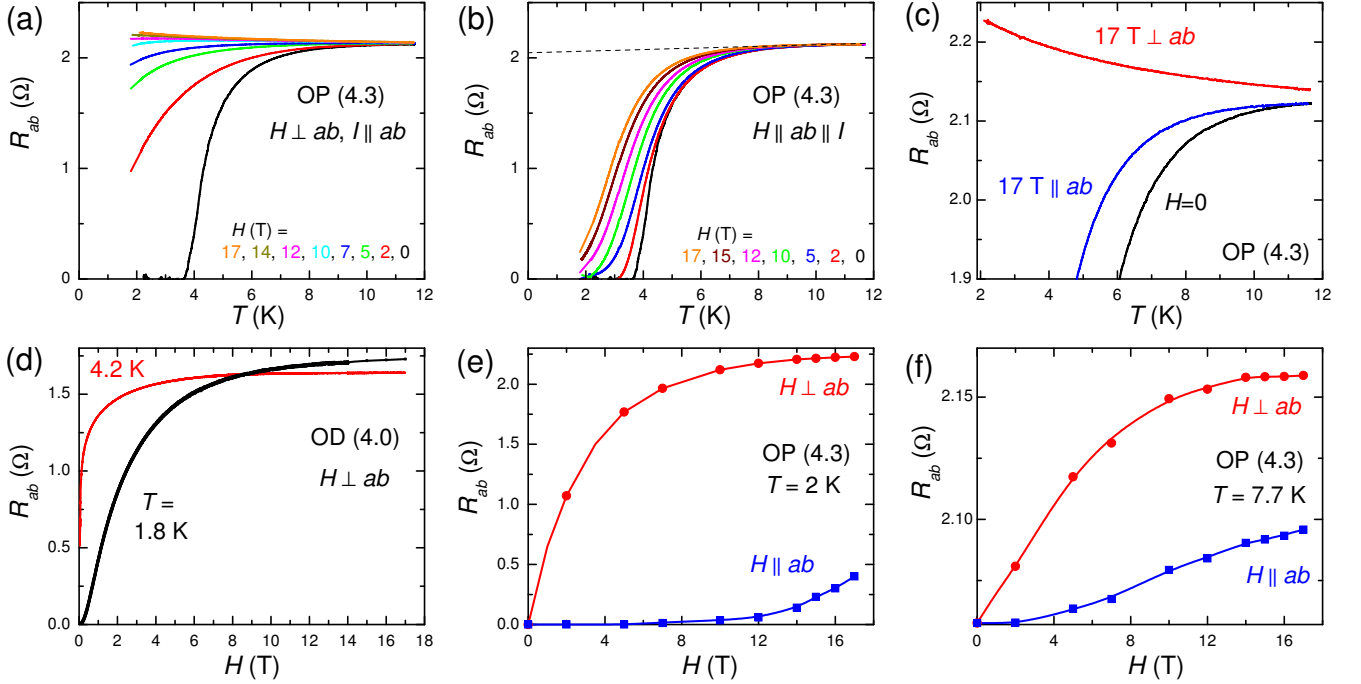


FIG. 2. (Color online) T -dependencies of the in-plane resistance at magnetic fields (a) perpendicular and (b) parallel to the ab -planes. (c) Comparison of the data from (a) and (b) for zero and 17 T. For $H \parallel ab$ the $R_{ab}(T)$ is shifted to lower temperatures. For $H \perp ab$ it is completely suppressed and R_{ab} is shifted upwards, indicating presence of a positive orbital magnetoresistance in the normal state. (d) MR in a perpendicular field below and just above T_c . Note that the saturation field $\sim H_{c2}(T)$ is decreasing with $T \rightarrow T_c$. Panels (e) and (f) show MR for both field orientations (e) below and (f) above T_c . The positive MR at $T > T_c$ is caused both by suppression of superconducting fluctuations and an additional orbital normal state MR.

doped crystal from the same batch (data from Ref. [30]). It is seen that at high fields $R_c(H^\perp)$ is approximately linear in the semi-logarithmic scale. An extrapolation to the normal resistance $R_n \sim 160\ \Omega$ yields the PG closing field $H^* \sim 300\ \text{T}$. It corresponds to the Zeeman energy $g\mu_B H^* \sim 35\ \text{meV} \simeq \Delta_{PG}$ [30].

C. Angular magnetoresistance at $T < T_c$

Angular dependence of the upper critical field $H_{c2}(\Theta)$ is given by the following equations:

$$\left(\frac{H_{c2}(\Theta) \sin \Theta}{H_{c2}^\perp}\right)^2 + \left(\frac{H_{c2}(\Theta) \cos \Theta}{H_{c2}^\parallel}\right)^2 = 1, \quad (1)$$

for a three-dimensional (3D) superconductor and

$$\left|\frac{H_{c2}(\Theta) \sin \Theta}{H_{c2}^\perp}\right| + \left(\frac{H_{c2}(\Theta) \cos \Theta}{H_{c2}^\parallel}\right)^2 = 1, \quad (2)$$

for the 2D case. In the simplest case of an isotropic superconductor the flux-flow resistivity can be approximately estimated from the Bardeen-Stephen model [62],

$$R(\Theta) = R_n \frac{H}{H_{c2}(\Theta)}. \quad (3)$$

It connects the angular MR $R(\Theta)$ with $H_{c2}(\Theta)$. The main qualitative difference between 3D and 2D cases is that $R(\Theta = 0^\circ)$ has a smooth minimum in the 3D case and a sharp cusp-like dip in the 2D case [63].

Figures 4 (a) and (b) show angular dependencies of the in-plane resistance $R_{ab}(\Theta)$ at $T = 2\ \text{K}$ measured upon rotation around two orthogonal axes in the ab -plane (a) perpendicular and (b) parallel to the current. In both cases $\Theta = 90^\circ$ corresponds to $H \perp ab, H \perp I$. But $\Theta = 0^\circ$, corresponds to either (a) the Lorentz force-free configuration $H \parallel I$, or (b) to the case $H \perp I$ when the Lorentz force is acting on Josephson vortices in the direction perpendicular to layers. Dashed lines in (b) represent properly scaled data from panel (a) [64]. It is seen that the behavior in both cases is very similar. Therefore, at $H \parallel ab$ the flux-flow contribution to R_{ab} is small either due to zero Lorentz force or a strong intrinsic pinning in the layered superconductor [65–67], which prevents motion of Josephson vortices across the planes.

Fig. 4 (c) shows angular dependencies of the c -axis resistance. Apart from the dip at $\Theta \sim 0^\circ$ due to the anisotropy of H_{c2} , the $R_c(\Theta)$ has an additional sharp

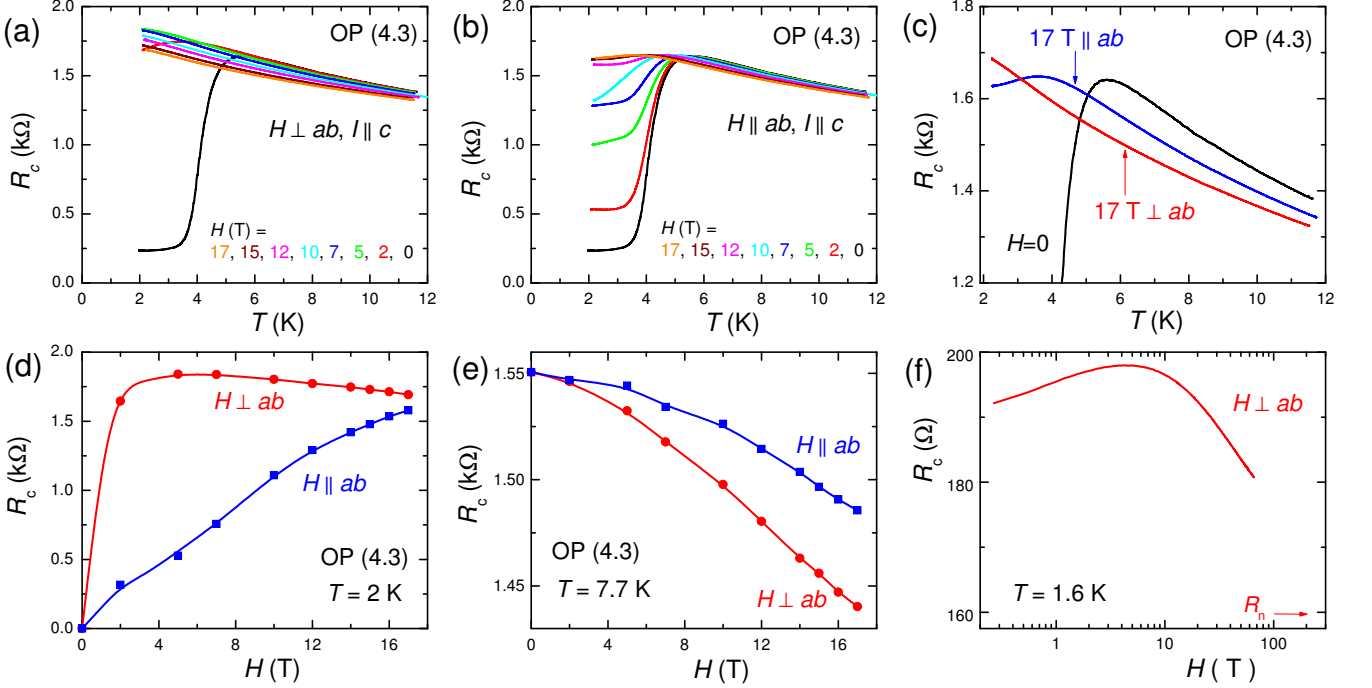


FIG. 3. (Color online) Temperature dependencies of the c -axis resistance for (a) $H \perp ab$ and (b) $H \parallel ab$. (c) Comparison of the data from (a) and (b) for $H = 0$ and 17 T. Panels (d) and (e) show c -axis MR for the two field orientations (d) below and (e) above T_c . It is seen the normal state negative MR is present for both field orientations. (f) $R_c(H^\perp)$ measured up to 65 T (data from Ref. [30]). It is seen that there is both a positive MR at low fields due to suppression of the supercurrent and a negative MR at high fields due to suppression of the PG.

maximum at $\Theta = 0^\circ$ due to onset of the Josephson flux-flow phenomenon [61]. In this case the Lorentz force is directed along the ab -planes and easily drags Josephson vortices with low pinning and viscosity [60]. The shape of $R_c(\Theta)$ at large angles is visibly affected by the negative normal state MR, which causes a shallow minimum of $R_c(\Theta)$ at $\Theta = 90^\circ$ at large fields.

From Figs. 4 (a-c) it is seen that $R(\Theta)$ exhibits a cusp at $\Theta = 0^\circ$, indicating the 2D-nature of superconductivity in CuO planes. The cusp becomes narrower and sharper with increasing field. This is in a qualitative agreement with calculations for the 2D model using Eqs.(2,3), shown in Fig. 4 (d). The sharpening of the cusp at $\Theta = 0^\circ$ occurs when the field becomes larger than H_{c2}^\perp . In this case the sample is in the normal state with a flat $R_{ab}(\Theta) = R_n$ for angles $\Theta \sim 90^\circ$ at which $H_{c2}(\Theta) < H$. As the field approaches H_{c2}^\parallel , superconductivity survives only in a narrow range of angles $\Theta \sim 0^\circ$. Therefore, a significant narrowing of the cusp at $H = 17$ T in Fig. 4 (a-c) indicates that H_{c2}^\parallel is close to 17 T.

The anisotropy of H_{c2} can be analyzed from comparison of angular-dependent $R(\Theta)$ with MR at the corresponding parallel $R(H^\parallel = H \cos(\Theta))$ and perpendicular $R(H^\perp = H \sin(\Theta))$ field orientations. If one of the field components is smaller than the corresponding H_{c2} , adding of an orthogonal component will contribute to

suppression of superconductivity. But if the field component is larger than H_{c2} , than an extra field component will not give a significant contribution to MR. In Figs. 4 (e) and (f) we perform such the comparison at $T = 2$ K. Black symbols in Figs. 4 (e) represent $R_{ab}(\Theta)$ at $H = 17$ T from Fig. 4 (a) as a function of $\sin^2(\Theta)$. The solid red line represents the MR in solely the perpendicular field component $R_{ab}[H^\perp = H \sin(\Theta)]$. The dashed blue line represents a sum of resistances in the corresponding perpendicular and parallel field components $R_{ab}[H^\perp = H \sin(\Theta)] + R_{ab}[H^\parallel = H \cos(\Theta)]$, shown in Fig. 2 (e). It is seen that at $\sin^2(\Theta) \gtrsim 0.35$ the angular MR is determined almost entirely by H^\perp and an additional H^\parallel does not contribute significantly to MR. This angle corresponds to $H^\perp = H \sin(\Theta) > H_{c2}^\perp \simeq 10$ T, as indicated by a vertical arrow in Fig. 4 (e). At larger angles superconductivity is already suppressed because $H^\perp > H_{c2}^\perp$ and MR becomes insensitive to an additional parallel field component. Such the analysis confirms that $H_{c2}^\perp \simeq 10$ T. At smaller angles $H^\perp < H_{c2}^\perp$ and H^\parallel does contribute to MR, although not additively.

Fig. 4 (f) represents a similar comparison for the out-of-plane resistance. Solid and dashed lines represent the MR solely in perpendicular and parallel fields from Fig. 3 (d). Apparently, $R_c(\Theta)$ is not determined by a single field component. The most pronounced feature of $R_c[\sin^2(\Theta)]$

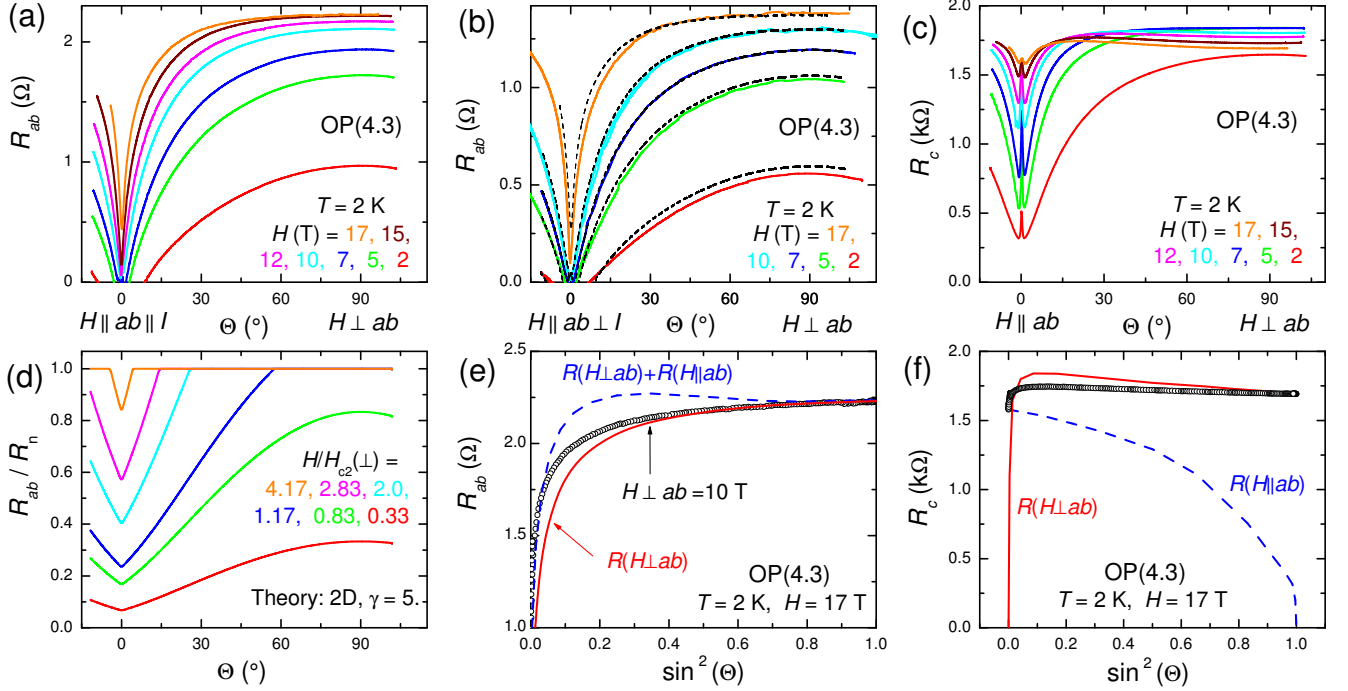


FIG. 4. (Color online) (a) and (b) Angular dependencies of in-plane resistances for rotation around two orthogonal axes in the ab -plane. Dashed lines in (b) represent scaled data from (a) [64]. (c) Angular dependence of the c -axis resistance. The peak at $\Theta = 0^\circ$ is due to onset of Josephson flux-flow. (d) Theoretical angular dependencies of flux-flow resistances for a 2D model with an anisotropy $\gamma = 5$. Note that the cusp at $\Theta = 0^\circ$ becomes sharper at $H > H_{c2}^\perp$ because superconductivity survives only in a narrow range of angles around $\Theta = 0^\circ$. A similar narrowing is seen in panels (a-c). Panels (e) and (f) represent comparison of (e) in-plane and (f) out-of-plane angular MR (symbols) with resistances at the corresponding perpendicular $H^\perp = H \sin(\Theta)$ (solid lines) and parallel $H^\parallel = H \cos(\Theta)$ field components at $T = 2$ K and $H = 17$ T.

is a rapid drop at $\sin(\Theta) \rightarrow 0$, which reflects the corresponding behavior of $R_c(H^\perp)$. Therefore, the crystal still maintains some superconductivity at $H^\parallel = 17$ T, but it is rapidly suppressed by a small additional H^\perp component upon a slight rotation of the crystal. Consequently, $H_{c2}^\parallel(2\text{K})$ is slightly larger than 17 T. On the other hand, since $H_{c2}^\perp < 17$ T, there is no similar drop at $\sin(\Theta) = 1$.

FLUCTUATION MAGNETORESISTANCE

From comparison of Figs. 4 (a), (b) and (d) it is clear that Eqs. (2) and (3) only explain the narrowing of the cusp, but do not fit the $R(\Theta)$ data. This demonstrates inappropriateness of Eq. (3) for layered superconductors because it does not take into consideration transformation of the vortex structure, the pinning strength and the Lorentz force upon rotation of the crystal. Furthermore, Eq. (3) assumes that the resistance always reaches the normal state value R_n at $H = H_{c2}$ and thus neglects the remaining fluctuation para-conductivity at $H > H_{c2}$ [33]. As discussed above, $R_{ab}(\Theta = 0^\circ)$ should have minimal flux-flow contribution either due to zero Lorentz force, or presence of a strong intrinsic pinning. Consequently, the dip in resistance at $\Theta = 0^\circ$ in Fig. 4 (a) and the major

part of the resistive transition $0 < R < R_n$ at $H \parallel ab \parallel I$ in Fig. 2 (b) are due to fluctuation conductivity, rather than flux-flow. Without flux-flow, H_{c2} would correspond to the onset of resistivity $R \sim 0$, rather than $R = R_n$. This has been demonstrated by simultaneous tunneling and transport measurements for conventional superconductors [16]. Without exact knowledge of the flux-flow contribution it is impossible to confidently extract H_{c2} from $R(T, H)$ data at $T < T_c$. The lack of criteria for $R(H = H_{c2})$ obscures estimation of H_{c2} [5]. Therefore, in the remaining part of the manuscript we will focus on the analysis of fluctuation part of MR at $T > T_c$. As we will demonstrate, such data do not suffer from ambiguity associated with flux-flow phenomenon and facilitate confident extraction of H_{c2} .

A. Angular magnetoresistance at $T > T_c$

Figure 5 (a) shows angular dependencies of the in-plane resistance at $H = 10$ T and at different T close and above $T_c \simeq 4.3$ K. Here $\Theta = 0^\circ$ corresponds to zero Lorentz force configuration $H \parallel ab \parallel I$. It is seen that the cusp at $\Theta = 0^\circ$, characteristic for the 2D superconducting state, is rapidly diminishing with increasing $T > T_c$. It

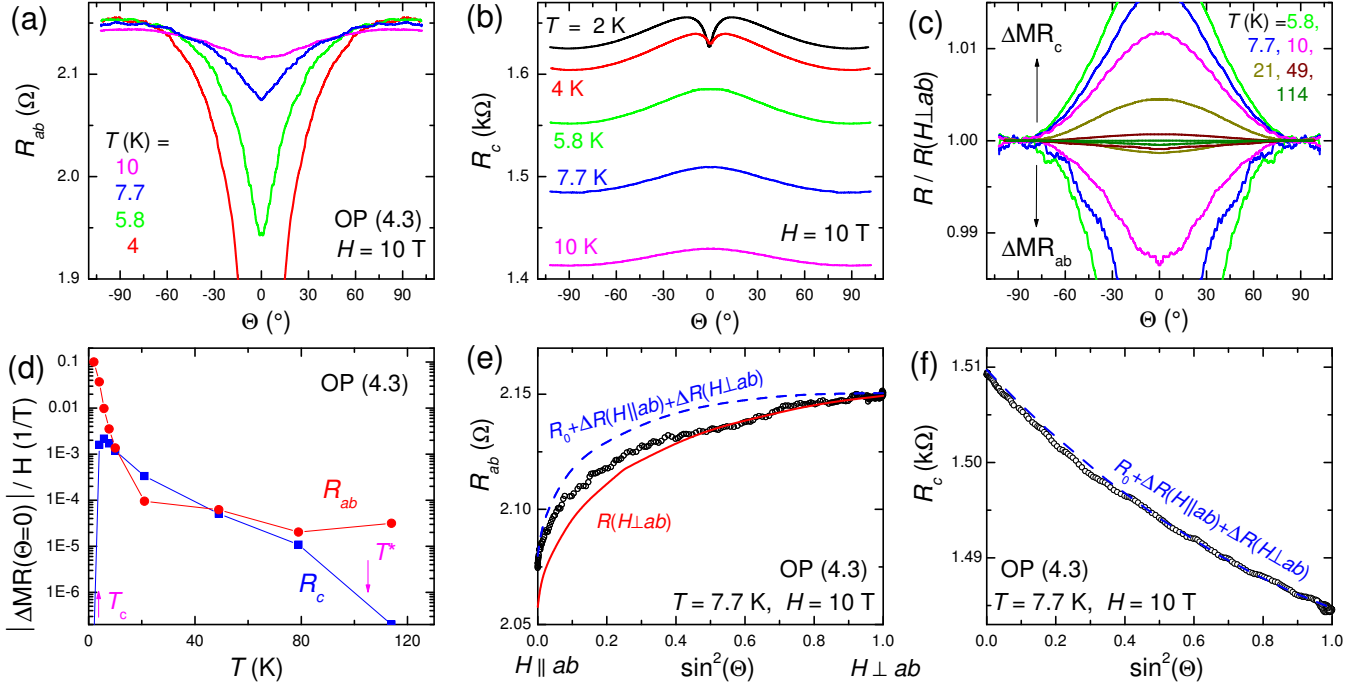


FIG. 5. (Color online) Angular dependence of (a) in-plane and (b) c -axis resistances at $H = 10$ T for different temperatures. The cusp at $\Theta = 0^\circ$ is vanishing at $T \gtrsim 2T_c$ for R_{ab} and at $T > T_c$ for R_c . (c) Angular dependent MR above T_c , normalized by $R(\Theta = 90^\circ)$. At $T \geq 10$ K the MR is varying in a smooth 3D-manner. (d) Temperature dependencies of absolute values of angular MR amplitudes normalized by the field (in the semi-logarithmic scale). Note that the in-plane MR decays at a scale $T \sim T_c$ and the out-of plane MR at the PG temperature $T^* \simeq 110$ K. Panels (e) and (f) represent comparison of (e) in-plane and (f) out-of-plane angular MR at $T = 7.7$ K $> T_c$ with the MR at the corresponding parallel and perpendicular field components. The in-plane angular MR at not too small angles is dominated by the perpendicular field component (solid line). The c -axis angular MR is given by the additive contribution of the two field components (dashed lines).

disappears at $\sim 2T_c$. At $T \gtrsim 10$ K it turns into a shallow minimum, which persists to $T \gg T_c$ and represents the anisotropy of the positive orbital MR in the normal state.

Fig. 5 (b) shows angular dependencies of the c -axis resistance below and above T_c . Here, measurements were performed at bias above the Josephson flux-flow branch in the I - V so that the Josephson flux-flow peak in $R_c(\Theta = 0^\circ)$ does not occur [61]. Above T_c the cusp in $R_c(\Theta) = 0^\circ$ completely disappears and only a shallow maximum at $\Theta = 0^\circ$ remains, which indicates a small angular anisotropy of the normal state MR, as seen from Fig. 3 (e). In Fig. 5 (c) we show angular dependencies of in-plane and c -axis resistances, normalized by the corresponding values at $\Theta = 90^\circ$. One can see a shallow 3D behavior in the normal state.

In Fig. 5 (d) we show absolute values of the angular MR amplitude $|\Delta MR(\Theta = 0^\circ) = R(0^\circ)/R(90^\circ) - 1|$, normalized by the magnetic field, for the in-plane and the c -axis resistances. The in-plane ΔMR_{ab} (circles) is large in the superconducting state and remains significant in the fluctuation region at $T_c < T \lesssim 2T_c$ when the cusp in $R_{ab}(\Theta = 0^\circ)$ is observed, see Fig. 5 (a). With increasing T , $|\Delta MR_{ab}|$ rapidly decreases. At $T > 20$ K it flattens off. The remaining weakly T -dependent value represents

the anisotropy of the positive in-plane MR in the normal state, presumably of the orbital origin. The out-of-plane $|\Delta MR_c|$ (squares) decreases almost exponentially with increasing temperature in a wide T -range above T_c . It becomes hardly detectable above the pseudogap opening temperature $T^* \simeq 110$ K, while the in-plane ΔMR_{ab} still remains recognizable.

A different behavior of in-plane and out-of-plane MR can be also seen from comparison of individual and combined contributions of the two field components. Symbols in Figs. 5 (e) and (f) show angular dependent (e) in-plane and (f) c -axis MR at $T = 7.7$ K $> T_c$ as a function of $\sin^2(\Theta)$. Dashed blue lines represent additive contributions from the two field components, $R = R_0 + \Delta R(H^\perp) + \Delta R(H^\parallel)$, where $R_0 = R(H = 0)$, and $\Delta R(H^\perp)$ and $\Delta R(H^\parallel)$ are the corresponding MR solely in perpendicular and parallel fields, shown in Figs. 2 (f) and 3 (e). It is seen that the c -axis MR is well described by the simple additive contribution of the two field components, while the in-plane does not. This reflects different mechanisms of in-plane and out-of-plane magnetoresistances. The negative c -axis MR is due to field suppression of the pseudogap. The applied field is much smaller than the PG closing field $H^* \sim 300$ T [30].

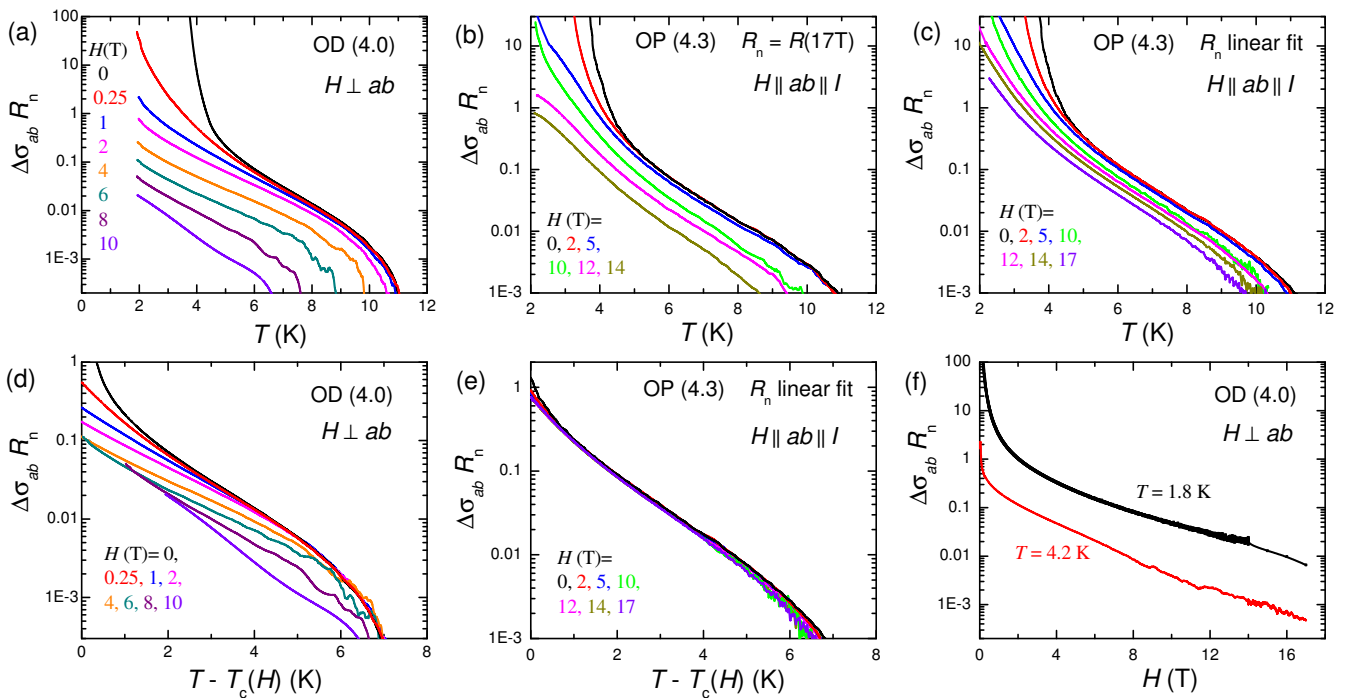


FIG. 6. (Color online) Fluctuation part of the in-plane conductivity $\Delta\sigma_{ab}(T) = 1/R_{ab}(T) - 1/R_n(T)$, normalized by the normal state resistance, for fields (a) perpendicular and (b,c) parallel to the ab -plane. Curves in panels (b) and (c) were obtained from the same data using different $R_n(T)$: (b) $R_n = R_{ab}(H = 17 \text{ T})$, (c) linear extrapolation from high T , shown by the dashed line in Fig. 2 (b). It is seen that fluctuation para-conductivity decays approximately exponentially with increasing T with an almost field independent slope. Panels (d) and (e) show data from (a) and (c), respectively, shifted by $T_c(H)$. (f) Field dependence of para-conductivity $\Delta\sigma_{ab}(H^\perp)$ at different T . An approximately exponential decay is seen.

Therefore, the c -axis MR is far from saturation and is approximately linear in field, leading to additive, independent from each other, contribution from the two field components.

The positive in-plane MR at $T_c < T \lesssim 2T_c$ is mostly due to suppression of superconducting fluctuations with the characteristic field $H_{c2}^\perp \sim 10 \text{ T}$, which is in the range of applied fields. This leads to saturation of MR and to non-additive contribution of the two field components. Unlike the normal state angular MR, which has a 3D character, as shown in Fig. 5 (c), superconducting fluctuations at $T_c < T \lesssim 2T_c$ remain quasi-2D, as seen from the cusp in $R_{ab}(\Theta = 0)$ in Fig. 5 (b). The solid line in Fig. 5 (e) indicates that at not too small angles the in-plane MR is determined by the c -axis field component.

B. Fluctuation conductivity

Fluctuation para-conductivity is seen as a tail of the in-plane resistive transitions from Figs. 2 (a) and (b) at $T_c < T \lesssim 10 \text{ K}$, in the same range where the cusp is seen in the angular MR, Fig. 5 (a). Figures 6 (a-c) represent normalized excess conductivities $\Delta\sigma_{ab}(T) = 1/R_{ab}(T) - 1/R_n(T)$, in perpendicular and

parallel magnetic fields. Here we used different approximations for R_n : (a) $R_n^\perp(T) = R_{ab}(T, H^\perp = 14 \text{ T})$, (b) $R_n^\parallel(T) = R_{ab}(T, H^\parallel = 17 \text{ T})$, and (c) a linear extrapolation from high T , shown by the dashed line in Fig. 2 (b).

It is seen that for both field orientations the fluctuation conductivity at $T > T_c$ decreases approximately linearly in the semi-logarithmic scale with almost field-independent slopes. This implies

$$\Delta\sigma_{ab}(T, H) \propto \exp[-a(T - T_c(H))], \quad (4)$$

where a is some constant. A similar exponential decay has been reported for other cuprates [16, 49, 68]. Even though such an exponential decay does not follow explicitly from theoretical analysis of fluctuation conductivity [33, 69], it allows an unambiguous determination of the characteristic temperature scale $T_c(H)$ from the relative shift of the curves along the T -axis with respect to the known $T_c(H = 0)$. Since the $\Delta\sigma_{ab}(T)$ curves in Figs. 6 (a-c) remain almost parallel at different H , such determination of $T_c(H)$ does not suffer from widening of the resistive transition, as in the flux-flow case at $T < T_c$ in Fig. 2 (a). Therefore, thus obtained $T_c(H)$ has the same degree of certainty as $T_c(H = 0)$.

Equation (4) suggests that $\Delta\sigma(T, H)$ curves could be

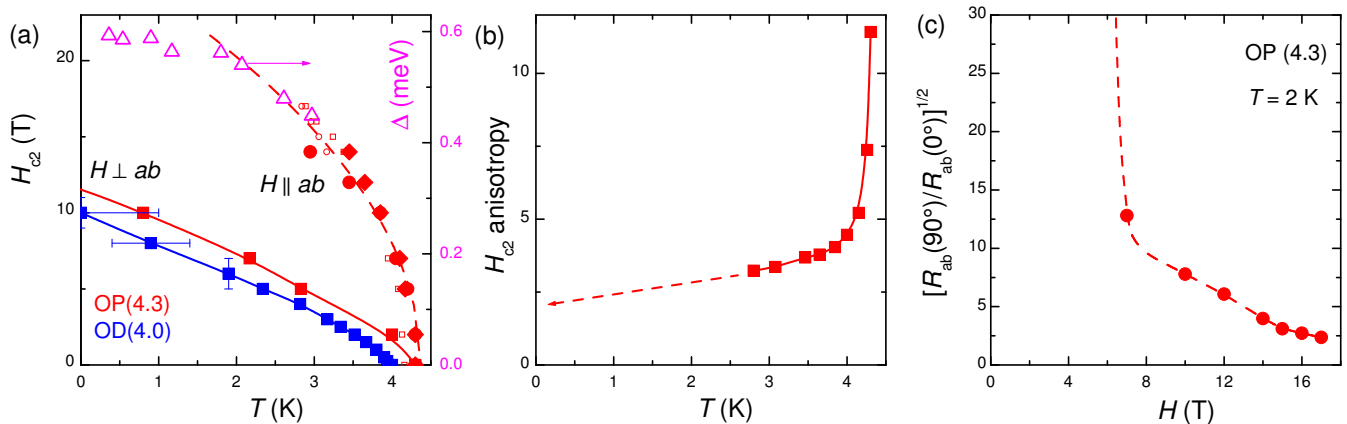


FIG. 7. (Color online) (a) The upper critical field perpendicular (filled squares) and parallel to layers (filled circles and rhombuses) obtained from the scaling analysis of fluctuation conductivity according to Eq. (4) at $T > T_c(H)$. For comparison we also show middle points $H_{50\%}(T)$ of in-plane (small open circles) and out-of-plane (small open squares) resistive transitions in parallel field. The dashed line represents the $\sqrt{T_c - T}$ dependence. Open triangles (right axis) show T -dependence of the superconducting gap, obtained by intrinsic tunneling spectroscopy [30]. (b) T -dependence of the anisotropy of the upper critical field $\gamma_H = H_{c2}^{\parallel}/H_{c2}^{\perp}$. It is seen that at low temperature it saturates at a small value $\gamma_H(0) \sim 2$. (c) Angular anisotropy of the in-plane resistance $R_{ab}(90^\circ)/R_{ab}(0^\circ)$ at $T = 2$ K as a function of magnetic field. The anisotropy rapidly decreases with increasing H as soon as the field approaches the paramagnetic limit.

collapsed in one by shifting them along the T -axis by $T_c(H)$. In Figs. 6 (d) and (e) we show such an attempt for the data from Figs. 6 (a) and (c), respectively. Even though the scaling is not always perfect, the shift parameter $T_c(H)$ is determined unambiguously because: (i) The shift for the curve at $H = 0$ is fixed by $T_c(0)$. (ii) The curves from low to intermediate fields do collapse at high enough T . (iii) When the curves do not collapse, we required that fluctuation conductivity for a given $T - T_c(H)$ should be decreasing with increasing H because superconductivity is suppressed by magnetic field. This means that the $\Delta\sigma(T - T_c(H))$ curves at higher H should always lie lower and should not cross the curves at smaller H . In Fig. 6 (d) the curve $\Delta\sigma(T, H = 10$ T) was not shifted at all, implying that $T_c(H = 10$ T) = 0, which is consistent with our previous estimation of $H_{c2}^{\perp}(T = 0) \simeq 10$ T.

Fig. 6 (f) represents a semi-logarithmic plot of $\Delta\sigma_{ab}R_n$ vs $H \perp ab$ for the OD(4.0) sample at $T = 1.8$ K and slightly above T_c at $T = 4.2$ K. It is seen that $\Delta\sigma_{ab}(H)$ decays almost exponentially also as a function of field at constant T . In this case the relative shift along the horizontal axis provides the characteristic magnetic field scale for suppression of superconductivity $\sim H_{c2}$. Assuming that $H_{c2} = 0$ at $T = 4.2$ K $\sim T_c$, we estimate from the relative shift of the two curves that $H_{c2}^{\perp}(T = 2$ K) $\simeq 6$ T. This is consistent with $T_c(H^{\perp} = 6$ T) $\simeq 2$ K, estimated from $\Delta\sigma_{ab}(T)$ scaling in Fig. 6 (d). Thus, from the analysis of fluctuation conductivity we obtain a confident estimation of $T_c(H)$ or equivalently $H_{c2}(T)$.

C. The upper critical field

Figure 7 (a) contains the main result of this work: T -dependencies of H_{c2} obtained from the analysis of fluctuation conductivity, Eq.(4), at $T > T_c(H)$ (filled symbols). Filled blue and red squares represent $H_{c2}^{\perp}(T)$ for OD(4.0) and OP(4.3) crystals, respectively. Horizontal and vertical error bars correspond to the accuracy of scaling of $\Delta\sigma(T, H)$ curves according to Eq. (4), as seen in Figs. 6 (d) and (f).

Estimation of H_{c2}^{\parallel} at low T is complicated by the lack of confident knowledge of $R_n(T)$. In Fig. 6 (b) and (c) we used two different approximations of $R_n(H^{\parallel})$. Filled circles and rhombuses represent $H_{c2}^{\parallel}(T)$ for the OP(4.3) crystal, obtained from the scaling of data in Fig. 6 (b) and Figs. 6 (c, f), respectively. Up to $H^{\parallel} = 10$ T both approximations of R_n give the same $H_{c2}^{\parallel}(T)$. Therefore, those values are confident. However, at $H > 12$ T results start to depend on the choice of $R_n(T)$. Unfortunately, none of the two approximations is good enough at $T \rightarrow 0$. Qualitatively, $R_n = R_{ab}(H^{\parallel} = 17$ T) tends to underestimate H_{c2}^{\parallel} because it assumes $H_{c2}^{\parallel}(T = 0) = 17$ T. The linear extrapolation of $R_n(T > T_c)$ tends to overestimate $H_{c2}^{\parallel}(T = 0)$ because it assumes that $R(H = H_{c2}) = R_n$. However, without the flux-flow phenomenon $R(H = H_{c2}) \simeq 0$ [16]. This is what we expect for our Lorentz force free data at $H \parallel ab$. In absence of a better way to define H_{c2}^{\parallel} at low T , in Fig. 7 (a) we also show fields $H_{50\%}(T)$ at which middle points of resistive transitions occurs for in-plane (open circles) and c -axis (open squares) resistances. Those points fall inbetween the un-

derestimating (solid circles) and overestimating (rhombuses) analysis of fluctuation conductivity. Therefore, they provide a reasonable estimate of H_{c2}^{\parallel} at lower T .

From Fig. 7 (a) it is seen that $H_{c2}^{\perp}(T)$ and $H_{c2}^{\parallel}(T)$ are qualitatively different. The $H_{c2}^{\perp}(T)$ is almost linear in the whole T -range $H_{c2}^{\perp}(T) \propto T_c - T$. Such a behavior is consistent with a conventional orbital upper critical field,

$$H_{c2}^{\perp} = \frac{\Phi_0}{2\pi\xi_{ab}^2}, \quad (5)$$

where Φ_0 is the flux quantum and ξ_{ab} is the in-plane coherence length, $\xi_{ab}(0) = 5.5 \pm 0.2$ nm.

The $H_{c2}^{\parallel}(T)$ is clearly non-linear. The dashed line in Fig. 7 (a) demonstrates that $H_{c2}^{\parallel}(T) \propto \sqrt{T_c - T}$. At the first glance, it resembles the behavior of $H_{c2}^{\parallel}(T)$ in thin film multilayers [65, 67],

$$H_{c2}^{\parallel} = \frac{\sqrt{3}\Phi_0}{\pi\xi_{ab}d}, \quad (6)$$

where d is the thickness of superconducting layers. However, the corresponding $d = 9.3 \pm 0.5$ nm is much larger than the thickness of CuO layers ~ 0.2 nm, as noted previously in Ref. [14], and is not connected to any geometrical length scale of the sample. Consequently, there is no agreement with Eq. (6).

D. The paramagnetic limit

The upper limit of H_{c2} is determined by Pauli paramagnetism. The spin-singlet pairing is destroyed when the Zeeman spin-split energy becomes comparable to the superconducting energy gap Δ . This gives [1, 34]

$$H_p = \frac{\sqrt{2}\Delta}{g\mu_B}, \quad (7)$$

where g is the gyromagnetic ratio and μ_B is the Bohr magneton. In case of negligible spin-orbit coupling $g \simeq 2$ this yields $dH_{c2}/dT(T = T_c) = -2.25$ T/K for d-wave superconductors [70]. Our values $H_{c2}^{\perp}/T_c \simeq 2.5$ T/K and $|dH_{c2}^{\perp}/dT|(T = T_c) \simeq 5$ T/K and especially $H_{c2}^{\parallel}/T_c \simeq 5$ T/K and $|dH_{c2}^{\parallel}/dT|(T = T_c) > 40$ T/K clearly exceed this limit. Most importantly, H_p does not depend on orientation of the field. Therefore, paramagnetically limited H_{c2} should be approximately isotropic, irrespective of the underlying effective mass anisotropy.

According to Eq.(7), H_p is determined solely by Δ . Open triangles in Fig. 7 (a) show $\Delta(T)$ -dependence measured by intrinsic tunneling spectroscopy on a slightly underdoped crystal from the same batch [30]. It matches nicely $H_{c2}^{\parallel}(T)$. Therefore, we conclude that the observed $H_{c2}^{\parallel}(T) \propto \sqrt{T_c - T}$ dependence is not originating from the geometrical confinement, Eq.(6), but follows the corresponding $\Delta(T)$ dependence of H_p in Eq.(7).

Fig. 7 (b) shows the anisotropy of the upper critical field $\gamma_H = H_{c2}^{\parallel}/H_{c2}^{\perp}$. Close to T_c it diverges due to different T -dependencies of the two fields. However, at $T \ll T_c$ it shows a tendency for saturation at $\gamma_H(T \rightarrow 0) \sim 2$. Such a low anisotropy of H_{c2} is remarkable for the layered Bi-2201 compound with $\gamma_m \sim 300$ [45].

In Fig. 7 (c) we show magnetic field dependence of the angular anisotropy $[R_{ab}(90^\circ)/R_{ab}(0^\circ)]^{1/2}$ obtained from the data in Fig. 4 (a). The anisotropy is large at low fields, but rapidly decreases at $H > 7$ T when the paramagnetic limitation starts to play a role. At high fields it tends to saturate at ~ 2 , consistent with γ_H in Fig. 7 (b). As mentioned above, paramagnetically limited H_{c2} should be isotropic. Therefore, a finite residual anisotropy $\gamma_H(T \rightarrow 0) \sim 2$ indicates that only H_{c2}^{\parallel} is paramagnetically limited, while H_{c2}^{\perp} is still governed by orbital effects. Finally we note that $\gamma_H < \gamma_m$ was reported for several unconventional superconductors [13, 14, 35, 36]. In particular, a nearly isotropic H_{c2} was reported for the (Ba,K)Fe₂As₂ pnictide [71] despite a quasi-2D electronic structure. It is likely that all those observations have the same origin.

CONCLUSIONS

To conclude, we presented a comprehensive analysis of both in-plane and out-of-plane magnetoresistance in a layered cuprate Bi_{2.15}Sr_{1.9}CuO_{6+ δ} with a low $T_c \simeq 4$ K. We have shown that the in-plane and the out-of-plane resistances behave differently almost in all respects. The in-plane magnetoresistance has two positive contributions. The positive in-plane MR due to suppression of superconductivity (or superconducting fluctuations) is dominant at $T \lesssim 2T_c$ and magnetic fields $H_{c2} \lesssim 10$ T. It is clearly distinguishable by its 2D cusp-like angular dependence. At $T \gtrsim 2T_c$ the superconducting contribution vanishes and only a weakly T -dependent positive MR, presumably of orbital origin, remains. Such normal state in-plane MR has a smooth 3D-type angular dependence. The c -axis MR at $T > T_c$ is dominated by a negative MR caused by suppression of the pseudogap. It decays rapidly upon approaching the PG opening temperature $T^* \simeq 110$ K $\gg T_c$ and at the PG closing field $H^* \sim 300$ T $\gg H_{c2}$, and exhibits a smooth 3D-type angular dependence. Different behavior of the in-plane and the out-of-plane MR underlines different origins of superconductivity and the c -axis pseudogap, which becomes particularly obvious from analysis of low- T_c cuprates [30].

The main focus of our work was on analysis of fluctuation conductivity at $T > T_c$. We observed a universal, nearly exponential, decay of in-plane para-conductivity as a function of temperature and magnetic field and proposed a method for extraction of H_{c2} based on a new type of a scaling analysis of the fluctuation para-conductivity.

This way we obtained confident values of H_{c2} , avoiding the complexity of flux-flow phenomena at $T < T_c$. We observed that H_{c2}^\perp is following a linear T -dependence $H_{c2}^\perp \propto 1 - T/T_c$, typical for H_{c2} limited by orbital effects. On the other hand, H_{c2}^\parallel follows the T -dependence of the superconducting gap with a characteristic $\propto \sqrt{1 - T/T_c}$ dependence close to T_c . Our main result is observation of a remarkably low anisotropy of the upper critical field $\gamma_H(T \rightarrow 0) \simeq 2$, which is much smaller than the effective mass anisotropy $\gamma_m \sim 300$. This demonstrates that the anisotropy of H_{c2} in unconventional superconductors may have nothing to do with the anisotropy of the electronic structure and the actual anisotropy of superconductivity at zero field. The large discrepancy in anisotropies serves instead as a robust evidence for paramagnetically limited superconductivity.

Acknowledgements

Technical support from the Core Facility in Nanotechnology at Stockholm University is gratefully acknowledged. We are grateful to A. Rydh and M.V. Kartsovnik for assistance in experiment and useful remarks.

* E-mail: Vladimir.Krasnov@fysik.su.se

† present address: Institut für Luft und Kältetechnik gemeinnützige Gesellschaft mbH, Bertolt-Brecht-Allee 20, D-01309 Dresden, Germany.

- [1] D. Saint-James, G. Sarma, and E.J. Thomas, Type-II superconductivity (Pergamon press 1969).
- [2] A. Gurevich, *Physica C* **456**, 160 (2007).
- [3] V.G. Kogan and R. Prozorov, *Rep. Prog. Phys.* **75**, 114502 (2012).
- [4] G. Blatter, M. V. Feigel'man, V. B. Geshkenbein, A. I. Larkin, and V. M. Vinokur, *Rev. Mod. Phys.* **66**, 1125 (1994).
- [5] S.I. Vedenev, A.G.M. Jansen, E. Haanappel, and P. Wyder, *Phys. Rev. B* **60**, 12467 (1999).
- [6] V.M. Krasnov, A. Yurgens, D. Winkler, P. Delsing and T. Claeson, *Phys. Rev. Lett.* **84**, 5860 (2000).
- [7] ØFischer, M. Kugler, I. Maggio-Aprile, and C. Berthod *Rev. Mod. Phys.* **79**, 353 (2007).
- [8] V.M. Krasnov, *Phys. Rev. B* **79**, 214510 (2009).
- [9] J.E. Hoffman, E. W. Hudson, K. M. Lang, V. Madhavan, H. Eisaki, S. Uchida, and J. C. Davis, *Science* **295**, 466 (2002).
- [10] A. Damascelli, Z.Hussain, and Z.X.Shen, *Rev. Mod. Phys* **75**, 473 (2003).
- [11] S.I. Ideta, T. Yoshida, A. Fujimori, H. Anzai, T. Fujita, A. Ino, M. Arita, H. Namatame, M. Taniguchi, Z.X. Shen, K. Takashima, K. Kojima, and S.I. Uchida, *Phys. Rev. B* **85**, 104515 (2012).
- [12] J. L. O'Brien, H. Nakagawa, A. S. Dzurak, R. G. Clark, B. E. Kane, N. E. Lumpkin, N. Miura, E. E. Mitchell, J. D. Goettee, J. S. Brooks, D. G. Rickel, and R. P. Starrett, *Phys. Rev. B* **61**, 1584 (2000).
- [13] T. Sekitani, N. Miura, S. Ikeda, Y.H. Matsuda, and Y. Shiohara, *Physica B* **346-347**, 319-324 (2004).
- [14] S. I. Vedenev, C. Proust, V.P. Mineev, M. Nardone, and G.L.J.A. Rikken, *Phys. Rev. B* **73**, 014528 (2006).
- [15] P. Li, F. F. Balakirev, and R. L. Greene, *Phys. Rev. B* **75**, 172508 (2007).
- [16] V.M. Krasnov, H. Motzkau, T. Golod, A. Rydh, S.O. Katterwe and A.B. Kulakov *Phys. Rev. B* **84**, 054516 (2011).
- [17] B. J. Ramshaw, J. Day, B. Vignolle, D. LeBoeuf, P. Dosanjh, C. Proust, L. Taillefer, R. Liang, W. N. Hardy, and D. A. Bonn, *Phys. Rev. B* **86**, 174501 (2012).
- [18] J. Chang, N. Doiron-Leyraud, O. Cyr-Choiniere, G. Grissonnanche, F. Laliberte, E. Hassinger, J-Ph. Reid, R. Daou, S. Pyon, T. Takayama, H. Takagi, and L. Taillefer, *Nature Phys.* **8**, 751 (2012).
- [19] G. Grissonnanche, et al., *Nature Comm.* **5**, 3280 (2014).
- [20] Y. Ando, A.N. Lavrov, and S. Komiya, *Phys. Rev. Lett.* **90**, 247003 (2003).
- [21] J.L. Tallon and J.W. Loram, *Physica C* **349**, 53 (2001).
- [22] I.M. Vishik, M. Hashimoto, R.H. He, W.S. Lee, F. Schmitt, D. Lu, R.G. Moore, C. Zhang, W. Meevasana, T. Sasagawa, S. Uchida, K. Fujita, S. Ishida, M. Ishikado, Y. Yoshida, H. Eisaki, Z. Hussain, T.P. Devereaux, and Z.X. Shen *PNAS* **109**, 18332 (2012).
- [23] F. Onufrieva and P. Pfeuty, *Phys. Rev. Lett.* **109**, 257001 (2012).
- [24] J.D. Sau, I. Mandal, S. Tewari, and S. Chakravarty, *Phys. Rev. B* **87**, 224503 (2013).
- [25] M.E. Simon and C.M. Varma, *Phys. Rev. Lett.* **89**, 247003 (2002).
- [26] C. Weber, A. Läuchli, F. Mila, and T. Giamarchi, *Phys. Rev. Lett.* **102**, 017005 (2009).
- [27] J. Orenstein and J.E. Moore, *Phys. Rev. B* **87**, 165110 (2013).
- [28] A.M. Gabovich and A.I. Voitenko, *Low. Temp. Phys.* **39**, 232 (2013).
- [29] T. Kawakami, T. Shibauchi, Y. Terao, M. Suzuki, and L. Krusin-Elbaum, *Phys. Rev. Lett.* **95**, 017001 (2005).
- [30] Th. Jacobs, S. O. Katterwe, H. Motzkau, A. Rydh, A. Maljuk, T. Helm, C. Putzke, E. Kampert, M. V. Kartsovnik, and V. M. Krasnov, *Phys. Rev. B* **86**, 214506 (2012).
- [31] A. Dubroka et al., *Phys. Rev. Lett.* **106**, 047006 (2011).
- [32] T. Kondo, Y. Hamaya, A.D. Palczewski, T. Takeuchi, J. S. Wen, Z.J. Xu, G. Gu, J. Schmalian and A. Kaminski, *Nature Phys.* **7**, 21 (2011).
- [33] A. Glatz, A.A. Varlamov and V.M. Vinokur, *Phys. Rev. B* **84**, 104510 (2011).
- [34] A.M. Clogston, *Phys. Rev. Lett.* **9**, 266 (1962).
- [35] F. Zuo, J.S. Brooks, R.H. McKenzie, J.A. Schlueter and J.M. Williams, *Phys. Rev. B* **61**, 750 (2000).
- [36] J.Singleton, *Rep. Prog. Phys.* **63**, 1111 (2000).
- [37] I.J. Lee, P.M. Chaikin, and M.J. Naughton, *Phys. Rev. B* **62**, R14669 (2000).
- [38] K. Cho, H. Kim, M. A. Tanatar, Y.J. Song, Y.S. Kwon, W.A. Coniglio, C.C. Agosta, A. Gurevich, and R. Prozorov, *Phys. Rev. B* **83**, 060502 (2011).
- [39] S. Khim, B. Lee, J.W. Kim, E.S. Choi, G.R. Stewart, and K.H. Kim, *Phys. Rev. B* **84**, 104502 (2011).
- [40] P. Burger, F. Hardy, D. Aoki, A. E. Böhmer, R. Eder, R. Heid, T. Wolf, P. Schweiss, R. Fromknecht, M. J. Jackson, C. Paulsen, C. Meingast, *Phys. Rev. B* **88**, 014517 (2013).

- [41] H. A. Radovan, N. A. Fortune, T. P. Murphy, S. T. Hannahs, E. C. Palm, S. W. Tozer, and D. Hall *Nature* **425**, 51 (2003).
- [42] K. Kakuyanagi, M. Saitoh, K. Kumagai, S. Takashima, M. Nohara, H. Takagi, and Y. Matsuda *Phys. Rev. Lett.* **94**, 047602 (2005).
- [43] Y. Matsuda and H. Shimahara, *J. Phys. Soc. Jap.* **76**, 051005 (2007).
- [44] A.I. Buzdin and J.P. Brison, *Europhys. Lett.* **35**, 707 (1996).
- [45] L. Ya. Vinnikov, A.G. Jukina, V.N. Zverev, A.D. Shovkun, and A.B. Kulakov, *Zh. Exp. Teor. Fiz.* **146** 2/0 (2014).
- [46] A.N. Lavrov, Y. Ando and S. Ono, *Europhys. Lett.* **57**, 267 (2002).
- [47] E. Sonder, B. C. Chakoumakos, and B.C. Sales, *Phys. Rev. B* **40**, 6872 (1989).
- [48] B. Liang, A. Maljuk and C.T. Lin, *Physica C* **361**, 156 (2001).
- [49] H. Luo, and H.H. Wen, *Phys. Rev. B* **89**, 024506 (2014).
- [50] A. Yurgens, D. Winkler, T. Claeson, S. Ono and Y. Ando *Phys. Rev. Lett.* **90**, 147005 (2003).
- [51] Y. Ando, G.S. Boebinger, A. Passner, N. L. Wang, C. Geibel, and F. Steglich, *Phys. Rev. Lett.* **77**, 2065 (1996).
- [52] T. Watanabe, T. Fujii, and A. Matsuda, *Phys. Rev. Lett.* **79**, 2113 (1997).
- [53] Y. Yamada, K. Anagawa, T. Shibauchi, T. Fujii, T. Watanabe, A. Matsuda, and M. Suzuki, *Phys. Rev. B* **68**, 054533 (2003).
- [54] R. Kleiner and P. Müller, *Phys.Rev.B* **49** 1327 (1994)
- [55] S.O. Katterwe and V.M. Krasnov, *Phys. Rev. B* **80**, 020502(R) (2009).
- [56] H. Kashiwaya, T. Matsumoto, H. Shibata, H. Eisaki, Y. Yoshida, H. Kambara, S. Kawabata and S. Kashiwaya, *Appl. Phys. Express* **3**, 043101 (2010).
- [57] J.M. Ziman, Principles of the Theory of Solids (Cambridge Univ. Press 1999).
- [58] N. Morozov, L. Krusin-Elbaum, T. Shibauchi, L. N. Bulaevskii, M. P. Maley, Yu. I. Latyshev, and T. Yamashita, *Phys. Rev. Lett.* **84**, 1784 (2000).
- [59] S.O. Katterwe, A. Rydh and V.M. Krasnov, *Phys. Rev. Lett.* **101**, 087003 (2008).
- [60] S.O. Katterwe, A. Rydh, H. Motzkau, A.B. Kulakov, and V.M. Krasnov, *Phys. Rev. B* **82**, 024517 (2010).
- [61] H. Motzkau, S.O. Katterwe, A.Rydh and V.M. Krasnov, *Physica C* **491**, 51-55 (2013).
- [62] J.Bardeen and M.J. Stephen, *Phys. Rev.* **140**, A1197 (1965).
- [63] M.J. Naughton, R.C. Yu, P.K. Davies, J.E. Fischer, R.V. Chamberlin, Z.Z. Wang, T.W. Jing, N.P. Ong, and P.M. Chaikin, *Phys. Rev. B* **38**, 9280 (1988).
- [64] Measurements in Figs. 4 (a) and (b) were made over different sections of the same OP(4.3) crystal, with approximately factor two difference in length, which leads to the corresponding difference in resistances.
- [65] M. Tachiki, and S. Takahashi, *Solid St. Commun.* **70**, 291 (1989).
- [66] W.K. Kwok, U.Welp, V.M. Vinokur, S. Fleshler, J. Downey, and G.W. Crabtree, *Phys. Rev. Lett.* **67**, 390 (1991).
- [67] V.M. Krasnov, A.E. Kovalev, V.A. Oboznov and N.F. Pedersen, *Phys. Rev. B* **54**, 15448 (1996).
- [68] F. Rullier-Albenque, H. Alloul, and G. Rikken, *Phys. Rev. B* **84**, 014522 (2011).
- [69] K.S. Tikhonov, G. Schwiete, and A.M. Finkelstein, *Phys. Rev. B* **85**, 174527 (2012).
- [70] J. P. Carbotte, *Rev. Mod. Phys.* **62**, 1027 (1990).
- [71] H.Q. Yuan, J. Singleton, F. F. Balakirev, S. A. Baily, G. F. Chen, J. L. Luo, and N. L. Wan, *Nature* **457**, 565 (2009).